iomac
International Operational Modal Analysis Conference

11th International Operational Modal Analysis Conference

20 - 23 May 2025 | Rennes, France

Identifiability Analysis of the Input Excitation of two Mechanical Systems using the Lie-derivative and the Empirical Gramian Method

M. Thing[1]
G. Abbiati[2]

[1] Department of Civil and Architectural Engineering, Aarhus University, 8000 Aarhus, Denmark, mlth@cae.au.dk
[3] Department of Civil and Architectural Engineering, Aarhus University, 8000 Aarhus, Denmark, abbiati@cae.au.dk

ABSTRACT
Input estimation indicates a class of algorithms to estimate the input excitation of a dynamical system based on output measurements and a model of the system. The feasibility of the estimation is conditioned on the identifiability of input. Noteworthy, identifiability entails that the response of the dynamical system is sensitive to a specific variable, and its effect is distinguishable from those of all other variables. This work explores two methods for assessing the identifiability of the input using two benchmark dynamical systems, which are simulated numerically. One method is based on the calculation of Lie derivatives and the other method is based on the calculation of Empirical Gramians. To verify the outcomes of the identifiability analysis, joint input estimation is computed for both systems using the Augmented Extended Kalman Filter.

Keywords: Input estimation, identifiability, Lie derivatives, empirical Gramians

1. INTRODUCTION

Input estimation indicates a class of algorithms to estimate the input excitation of a dynamical system based on output measurements and a model of the system. Several approaches have been proposed to estimate unknown inputs of dynamic systems. Algorithms based on a direct implementation into the Bayesian filters based on joint input-state estimation can be found in [1–5]. Algorithms that rely on multi-stage estimation approaches can be found [6–8]. Regardless the selected input estimation algorithm, the feasibility of the input estimation problem is conditioned to the identifiability of the input based on the observed output. Identifiability deals with the problem of assessing whether the identification of the parameters of a dynamical system from observed data is a well-posed problem [9]. Local identifiability assesses whether parameters can be uniquely estimated in the surroundings of a specific point of the state space, while global identifiability aims to cover the entire state space. In [10], coefficient evaluation and nonlinear differential equation transformation are proposed for global identifiability, but both become computationally expensive for large systems. Successive orthogonalization is applied in [11] to rank parameters in a nonlinear mechanical system for real-time estimation. The work in [12] introduces an identifiability index by estimating confidence intervals using the profile likelihood method. Empirical Gramians are proposed in [13, 14] to extend identifiability analysis to nonlinear systems. In the work of [9, 15, 16], Lie derivatives are utilized to study the local identifiability of biological and mechanical systems. The work of [17], utilizes singular value decomposition of the sensitivity matrix is used to study local identifiability. Comparative studies on some of these methods can be found in [10, 18, 19].

This paper compares two of the listed methods, namely, the Lie derivative (LD) method [15] and the empirical Gramian (EG) method [14] in relation to the identifiability of the input excitation for two mechanical systems. Both LD and EG methods are presented in Section 2. Numerical benchmarks are presented in Section 3. The results of the study are presented in Section 4. Section 5. summarizes the main findings and future outlooks.

2. IDENTIFIABILITY ANALYSIS METHODS

The following notation is used to describe a dynamical system equation of motion in state-space form,

$$\dot{\mathbf{x}} = \mathbf{f}(\mathbf{x}, \mathbf{p}) \, , \mathbf{y} = \mathbf{g}(\mathbf{x}, \mathbf{p}) \tag{1}$$

$\mathbf{x} \in \mathbb{R}^n$ is the system state, $\mathbf{p} \in \mathbb{R}^m$ is the input excitation, and $\mathbf{y} \in \mathbb{R}^r$ is the vector of output measurements. The functions $\mathbf{f}(\cdot, \cdot) \in \mathbb{R}^n$ is the state equation and $\mathbf{g}(\cdot, \cdot) \in \mathbb{R}^r$ is the output equation. Observability refers to the ability to reconstruct a system's internal states from output data, while identifiability determines whether system parameters can be uniquely estimated from observed data. In this work, we are concerned with the identifiability of $\mathbf{p}$ based on the output measurement $\mathbf{y}$. In this context, identifiability analysis is reformulated within the framework of augmented observability. This reformulation interprets identifiability as an extended form of observability. Therefore, the state of the system is augmented to include unknown inputs as additional state variables $\tilde{\mathbf{x}} = [\mathbf{x}\, \mathbf{p}]$ and the state-space model of Eq.(1) is reformulated as,

$$\tilde{\mathbf{f}}(\tilde{\mathbf{x}}) := \begin{bmatrix} \mathbf{f}(\mathbf{x}, \mathbf{p}) \\ \mathbf{0} \end{bmatrix} \, , \tilde{\mathbf{g}}(\tilde{\mathbf{x}}) := \mathbf{g}(\mathbf{x}, \mathbf{p}) \tag{2}$$

with the state-space equations as $\tilde{\mathbf{f}} \in \mathbb{R}^{n+m} = \mathbb{R}^p$ and $\tilde{\mathbf{g}} \in \mathbb{R}^r$.

2.1. Lie derivative method

The LD method originates from differential geometry. One can define a matrix constructed using LDs to analyse the observability and identifiability of a system. The LD is computed as the derivative of $\tilde{\mathbf{g}}(\tilde{\mathbf{x}})$ along the flow $\tilde{\mathbf{x}}(t)$, which expressed can be seen as

$$\mathcal{L}_f \tilde{\mathbf{g}}(\tilde{\mathbf{x}}) = \frac{\partial \tilde{\mathbf{g}}(\tilde{\mathbf{x}})}{\partial t} = \frac{\partial \tilde{\mathbf{g}}}{\partial \tilde{\mathbf{x}}} \frac{\partial \tilde{\mathbf{x}}}{\partial t} = \frac{\partial \tilde{\mathbf{g}}}{\partial \tilde{\mathbf{x}}} \tilde{\mathbf{f}} \, (\tilde{\mathbf{x}}) \tag{3}$$

The second-order LD expression reads,

$$\mathcal{L}_f^2\tilde{\mathbf{g}}(\tilde{\mathbf{x}}) = \mathcal{L}_f(\mathcal{L}_f\tilde{\mathbf{g}}(\tilde{\mathbf{x}})) = \frac{\partial}{\partial\tilde{\mathbf{x}}}\left(\frac{\partial\tilde{\mathbf{g}}}{\partial\tilde{\mathbf{x}}}\tilde{\mathbf{f}}\left(\tilde{\mathbf{x}}\right)\right)\tilde{\mathbf{f}}\left(\tilde{\mathbf{x}}\right) \tag{4}$$

and higher-order LD expressions can be easily extrapolated. Is it clear from (4) that the symbolic complexity of LDs grows quickly for C^∞ due to the chain rule. The expression of the augmented observability matrix reads,

$$\boldsymbol{\mathcal{O}}_{LD}(\tilde{\mathbf{x}}) = \left[\frac{\partial}{\partial\tilde{\mathbf{x}}}\mathcal{L}_f^0\tilde{\mathbf{g}}(\tilde{\mathbf{x}}) \quad \frac{\partial}{\partial\tilde{\mathbf{x}}}\left(\mathcal{L}_f\tilde{\mathbf{g}}(\tilde{\mathbf{x}})\right) \quad \frac{\partial}{\partial\tilde{\mathbf{x}}}\left(\mathcal{L}_f^2\tilde{\mathbf{g}}(\tilde{\mathbf{x}})\right) \quad \cdots \quad \frac{\partial}{\partial\tilde{\mathbf{x}}}\left(\mathcal{L}_f^{p-1}\tilde{\mathbf{g}}(\tilde{\mathbf{x}})\right)\right]^\top \tag{5}$$

where $\mathcal{L}_f^0\tilde{\mathbf{g}}(\tilde{\mathbf{x}}) = \tilde{\mathbf{g}}(\tilde{\mathbf{x}})$. The Generalized Observability-Identifiability Rank Condition (OIRC) is determined by computing the rank of the matrix $\boldsymbol{\mathcal{O}}_{LD}(\tilde{\mathbf{x}})$ of Eq. (5), which defines local observability of the system. Specifically, if the matrix is full rank, it means that the augmented state $\tilde{\mathbf{x}}$ is fully observable from the output measurement $\mathbf{y}$.

2.2. Empirical Gramian method

The EG method described in [14] builds upon the definition of the empirical observability Gramian matrix described in [20]. The augmented observability matrix is computed using output trajectories produced by perturbing the initial conditions of the augmented state of the system as,

$$\boldsymbol{\mathcal{O}}_{EG}(\tilde{\mathbf{x}}) = \frac{1}{n_l}\sum_{l=1}^{n_l}\frac{1}{d_l^2}\int_0^\infty \boldsymbol{\Psi}^l(t)\,dt, \tag{6}$$

Each single scalar component of matrix $\boldsymbol{\Psi}^l(t)$ is defined as,

$$\Psi_{ij}^l(t) = \Psi_{ji}^l(t) = (\mathbf{y}^{l_i}(t) - \bar{\mathbf{y}}^{l_i})^\top(\mathbf{y}^{l_j}(t) - \bar{\mathbf{y}}^{l_j}) \tag{7}$$

where $\mathbf{y}^{l_i}(t)$ and $\mathbf{y}^{l_j}(t)$ is the output response vectors of the dynamical system computed for the augmented state perturbations of indices l_i and l_j, respectively, with $i, j \in \{1, \ldots, p\}$; $\bar{\mathbf{y}}^{l_i}$ and $\bar{\mathbf{y}}^{l_j}$ their time-averaged values. As one can see from (6), n_l sets of perturbations are taken, each one associated with a characteristic amplitude d_l. The reason for that is the dynamical system response manifold is typically amplitude-dependent. In this work, augmented state perturbations and their characteristic amplitude are computed using the Python toolbox freely available at [21]. The OIRC is determined by computing the rank of the augmented observability matrix $\boldsymbol{\mathcal{O}}_{EG}(\tilde{\mathbf{x}})$ of Eq. (6), which defines the local observability of the system. Specifically, if the matrix is full rank, it means that the augmented state $\tilde{\mathbf{x}}$ is fully observable from the output measurement $\mathbf{y}$.

3. NUMERICAL BENCHMARKS

The LD and EG methods are benchmarked on two numerical models, namely, a 3-DOF spring-mass system (3D-SM) and a 5-DOF simplified MBD model of a wind turbine (5D-WT). Figure 1 depicts both models. Model parameters are given in the respective subsections.

3.1. 3-DOF spring-mass system

The equation of motion of the 3D-SM model of Figure 1a is reported herein in state-space form,

$$\dot{\mathbf{x}} = \mathbf{f}\left(\mathbf{x}, \mathbf{p}\right) := \begin{bmatrix} \dot{q}_1 \\ \dot{q}_2 \\ \dot{q}_3 \\ -\begin{bmatrix} m_b & 0 & 0 \\ 0 & m_b & 0 \\ 0 & 0 & m_t \end{bmatrix}^{-1} \begin{bmatrix} p_1 + k_b(q_1 - q_3) + c_b\dot{q}_1 \\ p_2 + k_b(q_2 - q_3) + c_b\dot{q}_2 \\ k_b(-q_1 - q_2 + 2q_3) + k_t q_3 + k_t q_3^3 + c_t\dot{q}_3 \end{bmatrix} \end{bmatrix} \tag{8}$$

where $\mathbf{x} = [\mathbf{q}, \dot{\mathbf{q}}]^\top$ is the state vector and $\mathbf{p}$ is the vector of the applied loading, which is random with a mean around $100\,\mathrm{N}$ for an identical load, and random with the two means of $110\,\mathrm{N}$ and $95\,\mathrm{N}$ for different loadings. The stiffness parameter values are $k_b = 7.2 \times 10^3\,\mathrm{N/m}$ and $k_t = 7.2 \times 10^4\,\mathrm{N/m}$, the mass

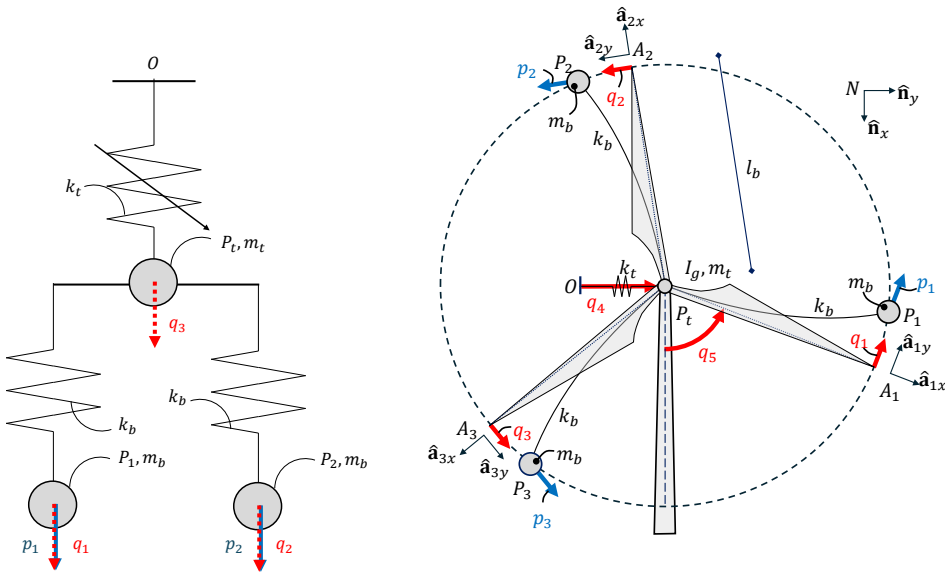

Figure 1: a) 3D-SM spring-mass system b) 5D-WT simplified wind turbine system.

parameter values are $m_b = 1.96\,\mathrm{kg}$ and $m_t = 10\,\mathrm{kg}$ and the mass-proportional damping coefficient value is $\alpha = 1\,\mathrm{s}^{-1}$. The output equation of the model have the following forms,

$$\mathbf{y}_a = \mathbf{g}(\mathbf{x}, \mathbf{p}) := \begin{bmatrix} q_2 & q_3 \end{bmatrix}^\top \tag{9}$$

$$\mathbf{y}_b = \mathbf{g}(\mathbf{x}, \mathbf{p}) := \begin{bmatrix} \ddot{q}_1 & \ddot{q}_3 \end{bmatrix}^\top \tag{10}$$

$$\mathbf{y}_c = \mathbf{g}(\mathbf{x}, \mathbf{p}) := \begin{bmatrix} \ddot{q}_3 \end{bmatrix}^\top \tag{11}$$

In order to distinguish between the three settings for the output, this case study is referred to as 3D-SM-a (-b/-c) in the result section.

3.2. 5-DOF wind turbine model

The 5D-WT model represents a wind turbine in a simplified manner. The model is characterized by 5 DOF $\{q_1, q_2, q_3, q_4, q_5\}$; $\{q_1, q_2, q_3\}$ coincides with the tip deflection of each blade, which is offset by a fixed angle $\Psi_1 = 0°, \Psi_2 = 120°, \Psi_3 = 240°$; q_4 represent the tower deflection and q_5 represent the hub rotation. The active and inertia forces for points P_1, P_2, P_3 are derived as;

$$\mathbf{f}^{P_i} = m_b g \mathbf{n}_z + p_i \mathbf{a}_{iz} - k_b q_i \mathbf{a}_{iz} - c_b \dot{q}_i \mathbf{a}_{iz} \quad \text{and} \quad \mathbf{f}^{P_i^*} = -m_b {}^N\mathbf{a}^{P_i}, \quad \text{for } (i = 1, 2, 3) \tag{12}$$

Similar to the other system, is the stiffness parameter values $k_b = 7.2 \times 10^3\,\mathrm{N/m}$ and $k_t = 7.2 \times 10^4\,\mathrm{N/m}$, the mass parameter values $m_b = 1.96\,\mathrm{kg}$ and $m_t = 10\,\mathrm{kg}$ and the mass-proportional damping is $c_b = m_b \cdot 1\,\mathrm{s}^{-1}$ and $c_t = m_t \cdot 1\,\mathrm{s}^{-1}$. In addition to active and inertia forces, this system will introduce active and inertia torques applied to frame A_1 from the rotor motion, where the contribution of the blades is summed up.

$$\mathbf{t}^{A_1} = -\left(\sum_{i=1}^{n_b} k_b l_b q_i + c_b l_b \dot{q}_i \right) \mathbf{n}_z - d_g \dot{q}_5 \mathbf{n}_z \tag{13}$$

$$\mathbf{t}^{A_1^*} = -\mathbf{I}^{A_1} \cdot {}^N\boldsymbol{\alpha}^{A_1} - {}^N\boldsymbol{\omega}^{A_1} \times \left(\mathbf{I}^{A_1} \cdot {}^N\boldsymbol{\omega}^{A_1} \right) \tag{14}$$

where $\mathbf{I}^{A_1} = I_g \hat{\mathbf{a}}_{1z} \otimes \hat{\mathbf{a}}_{1z}$ is the inertia dyadic and $d_g = 100\,\mathrm{Nms}$ is the damping from the generator along with $d_g = 0.1\,\mathrm{kgm}^2$. The length of the blades is $0.5\,\mathrm{m}$. The equation of motion (15) is subsequently computed by projecting the active and inertia forces/torques onto each partial velocity direction,

$${}^N\mathbf{v}_j^{P_t} \cdot \mathbf{f}^{P_t} + \sum_{i=1}^{3} {}^N\mathbf{v}_j^{P_i} \cdot (\mathbf{f}^{P_i} + \mathbf{f}^{*P_i}) + {}^N\boldsymbol{\omega}_j^{A_1} \cdot (\mathbf{t}^{A_1} + \mathbf{t}^{*A_1}) = 0 \quad (j = 1, 2, 3, 4, 5) \tag{15}$$

where the generalized velocities are obtained as partial derivatives of point velocities and frame angular velocities w.r.t. the generalized velocities $\dot{q}_j$,

$$ {}^{N}\mathbf{v}_j^{P_t} = \frac{\partial {}^{N}\mathbf{v}^{P_t}}{\partial \dot{q}_j} \quad , \quad {}^{N}\mathbf{v}_j^{P_i} = \frac{\partial {}^{N}\mathbf{v}^{P_i}}{\partial \dot{q}_j} \quad , \quad {}^{N}\boldsymbol{\omega}_j^{A_1} = \frac{\partial {}^{N}\boldsymbol{\omega}^{A_1}}{\partial \dot{q}_j} \tag{16} $$

To recast (15) in state-space form, a discrepancy function $\boldsymbol{\varepsilon}$ is introduced

$$ \boldsymbol{\varepsilon}(\mathbf{q}, \dot{\mathbf{q}}, \ddot{\mathbf{q}}, \mathbf{p}) = \begin{bmatrix} {}^{N}\mathbf{v}_1^{P_t} \cdot \mathbf{f}^{P_t} + \sum_{i=1}^{3} {}^{N}\mathbf{v}_1^{P_i} \cdot (\mathbf{f}^{P_i} + \mathbf{f}^{P_i^*}) + {}^{N}\boldsymbol{\omega}_1^{A_1} \cdot (\mathbf{t}^{A_1} + \mathbf{t}^{A_1^*}) \\ \vdots \\ {}^{N}\mathbf{v}_5^{P_t} \cdot \mathbf{f}^{P_t} + \sum_{i=1}^{3} {}^{N}\mathbf{v}_5^{P_i} \cdot (\mathbf{f}^{P_i} + \mathbf{f}^{P_i^*}) + {}^{N}\boldsymbol{\omega}_5^{A_1} \cdot (\mathbf{t}^{A_1} + \mathbf{t}^{A_1^*}) \end{bmatrix} \tag{17} $$

where $\mathbf{q} = \{q_1, q_2, q_3, q_4, q_5\}$ contains generalized position and $\mathbf{p}$ are the input parameters to estimate. For this specific problem, $\mathbf{p}$ can be either identical, or have three different configurations with means of $110\,\mathrm{N}$, $95\,\mathrm{N}$ and $90\,\mathrm{N}$. Starting from (17), the generalized mass and restoring force of the dynamic system are obtained as,

$$ \mathbf{M}(\mathbf{q}, \dot{\mathbf{q}}) = \frac{\partial \boldsymbol{\varepsilon}}{\partial \ddot{\mathbf{q}}} \quad , \quad \mathbf{g}(\mathbf{q}, \dot{\mathbf{q}}, \mathbf{p}) = \boldsymbol{\varepsilon}(\mathbf{q}, \dot{\mathbf{q}}, \dot{\mathbf{u}}, \mathbf{p}) - \mathbf{M}(\mathbf{q}, \dot{\mathbf{q}})\, \ddot{\mathbf{q}} \tag{18} $$

Generalized mass and restoring force are used to formulate the equation of motion in state-space form as,

$$ \dot{\mathbf{x}} = \mathbf{f}(\mathbf{x}, \mathbf{p}) := \begin{bmatrix} \mathbf{u} \\ -\mathbf{M}(\mathbf{q}, \mathbf{u})^{-1} \mathbf{g}(\mathbf{q}, \mathbf{u}, \mathbf{p}) \end{bmatrix} \tag{19} $$

where $\mathbf{u} = \dot{\mathbf{q}}$ and $\mathbf{x} = [\mathbf{q}, \mathbf{u}]^T$ is the state vector of the dynamic system. The full derivation of the model can be found in [22]. The output measurements of the system coincide with the tip of each blade and the top of the tower as the displacements and accelerations. The following three output settings are considered:

$$ \mathbf{y}_a = \mathbf{g}(\mathbf{x}, \mathbf{p}) := \begin{bmatrix} q_2 & q_3 & q_4 \end{bmatrix}^\top \tag{20} $$

$$ \mathbf{y}_b = \mathbf{g}(\mathbf{x}, \mathbf{p}) := \begin{bmatrix} {}^{N}\mathbf{a}^{P_1} \cdot \hat{\mathbf{a}}_{1y} & {}^{N}\mathbf{a}^{P_2} \cdot \hat{\mathbf{a}}_{2y} & {}^{N}\mathbf{a}^{P_3} \cdot \hat{\mathbf{a}}_{3y} & {}^{N}\mathbf{a}^{P_t} \cdot \hat{\mathbf{n}}_y \end{bmatrix}^\top \tag{21} $$

$$ \mathbf{y}_c = \mathbf{g}(\mathbf{x}, \mathbf{p}) := \begin{bmatrix} {}^{N}\mathbf{a}^{P_1} \cdot \hat{\mathbf{a}}_{1y} & {}^{N}\mathbf{a}^{P_3} \cdot \hat{\mathbf{a}}_{3y} & {}^{N}\mathbf{a}^{P_t} \cdot \hat{\mathbf{n}}_y \end{bmatrix}^\top \tag{22} $$

This case study is referred to as 5D-WT-a (-b/-c) in the result section.

4. RESULTS AND DISCUSSIONS

The identifiability of the input vector $\mathbf{p}$ of two systems have been analyzed using both the LD and EG methods considering the three different settings, namely, *a*, *b* and *c*. The EG method is applied on response history data characterized by a time span of $20\,\mathrm{s}$ and time step $0.01\,\mathrm{s}$; the specific setting of the EG method is given by $n_l = 4$ and $d_l = \{0.001, 0.01, 0.1, 1.0\}$. The main results of the comparison are the OIRCs and the computational time associated with their calculation, which are reported in Tables 1 and 2.

Table 1: Results of the identifiability analysis for 3D-SM with $p_1 = p_2$ and 5D-WT with $p_1 = p_2 = p_3$.

Label	**Full rank**	**EG method**		**LD method**	
		rank($\mathcal{O}_{EG}$)	CPU	rank($\mathcal{O}_{LD}$)	CPU
3D-SM-a	7	7	41s	7	54 min 24s
3D-SM-b	7	7	45s	7	91 min 47s
3D-SM-c	7	6	46s	6	65 min 21s
5D-WT-a	11	11	13 min 25 s	—	—
5D-WT-b	11	11	11 min 58s	—	—
5D-WT-c	11	11	13 min 51s	—	—

Tables 1 and 2 show that the OIRCs obtained from LD and EG on the 3D-SM model are consistent. Memory limitations have systematically prevented the application of the LD method to the 5D-WT model. The explanation is that when the equation of motion is C^{∞}, the complexity of the symbolic expression of the Lie derivatives saturates the available RAM. A standard laptop with 13$^{\text{th}}$ Gen Intel(R) Core$^{\text{TM}}$ i5-1345U 1.60 GHz processor and 16 GB RAM was used to perform the calculations. As can be observed in Table 1, when a single input is applied, the augmented state is fully observable for 5 out of the 6 cases. When the independent input are applied, as can be observed from Table 2, the rank of the augmented observability matrix tend to decrease.

Table 2: Results of the identifiability analysis for 3D-SM with $p_1 \neq p_2$ and 5D-WT with $p_1 \neq p_2 \neq p_3$.

Label	**Full rank**	**EG method**		**LD method**	
		rank($\mathcal{O}_{EG}$)	CPU	rank($\mathcal{O}_{LD}$)	CPU
3D-SM-a	8	8	1 min 8s	—	—
3D-SM-b	8	7	1 min 9s	—	—
3D-SM-c	8	6	1 min 13s	—	—
5D-WT-a	13	11	14 min 9s	—	—
5D-WT-b	13	13	17 min 30s	—	—
5D-WT-c	13	12	23 min 11s	—	—

As a final verification of the results of the identifiability analysis, the Augmented Extended Kalman Filter (AEKF) is applied to estimate the augmented state of both models for some of the output settings. For the implementation of the filter see [3], where the algorithm is shown. In all cases, input loading histories are low-pass filtered white noise. For the 5D-WT model, AEKF initial covariance matrices are,

$$\mathbf{P} = \begin{bmatrix} \mathbf{I}_{5\times5} \cdot 1 \times 10^{-5} & \mathbf{0} & \mathbf{0} \\ \mathbf{0} & \mathbf{I}_{5\times5} \cdot 1 \times 10^{-12} & \mathbf{0} \\ \mathbf{0} & \mathbf{0} & \mathbf{I}_{m\times m} \cdot 5 \times 10^{-2} \end{bmatrix}$$

$$\mathbf{Q} = \begin{bmatrix} \mathbf{I}_{10\times10} \cdot 1 \times 10^{-7} & \mathbf{0} \\ \mathbf{0} & \mathbf{I}_{m\times m} \cdot 5 \times 10^{-1} \end{bmatrix} \text{ and } \mathbf{R} = \mathbf{I}_{r\times r} \cdot 5 \times 10^{-3}$$

The results of the input estimation are reported in Figure 2. Specifically, Figure a refer to the case 5D-WT-b, where the rank of the augmented observability matrix is deficient. As can be appreciated, the estimation input does not converge to the true value. Figure b refer to the same case, where the rank of the augmented observability matrix is full. As can be appreciated, the estimation input converges to the true value.

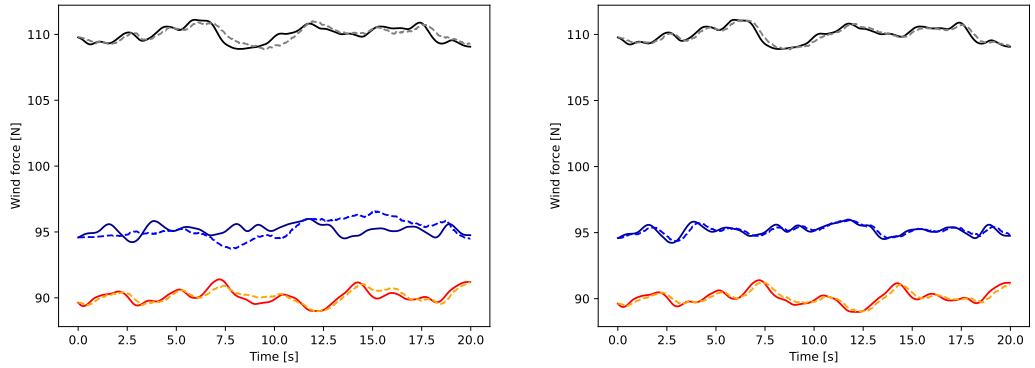

(a) **(b)**

Figure 2: Input estimation performed using the AEKF with the a) 5D-WT-b model and d) 5D-WT-a model for the case of $p_1 \neq p_2 \neq p_3$.

5. CONCLUSIONS

This paper benchmarked two approaches for identifiability analysis, namely, the Empirical Gramian method and the Lie derivative method, in relation to the estimation of the input excitation on two dynamical systems. The Empirical Gramian method allowed the study of the identifiability of both benchmark problems for all cases. However, the results obtained with the Empirical Gramian method might be affected by the specific selection of the perturbation parameters n_l and d_l. The Lie Derivative method does not have hyper-parameters, so it is, in principle, more objective. However, the Lie derivative method quickly saturates the computer RAM for a relatively small size of the augmented state if the equation of motion is nonlinear. The results of the analysis are consistent with the performance of the input estimation conducted with an AEKF. It is important to note that this is a preliminary study; therefore, our implementation of the LD method might be optimized further. This will be the subject of our future work.

REFERENCES

[1] Steven Gillijns and Bart De Moor. Unbiased minimum-variance input and state estimation for linear discrete-time systems with direct feedthrough. Automatica, 43(5):934–937, 2007. ISSN 0005-1098.

[2] Chien-Shu Hsieh. Extension of unbiased minimum-variance input and state estimation for systems with unknown inputs. Automatica, 45(9):2149–2153, 2009. ISSN 0005-1098.

[3] E. Lourens, E. Reynders, G. De Roeck, G. Degrande, and G. Lombaert. An augmented kalman filter for force identification in structural dynamics. Mechanical Systems and Signal Processing, 27:446–460, 2012.

[4] V.K. Dertimanis, E.N. Chatzi, S. Eftekhar Azam, and C. Papadimitriou. Input-state-parameter estimation of structural systems from limited output information. Mechanical Systems and Signal Processing, 126:711–746, 2019. ISSN 0888-3270.

[5] Bernard Delyon and Qinghua Zhang. On the optimality of the kitanidis filter for state estimation rejecting unknown inputs. Automatica, 132:109793, 2021.

[6] Peter K Kitanidis. Unbiased minimum-variance linear state estimation. Automatica, 23(6):775–778, 1987.

[7] Qinghua Zhang and Liangquan Zhang. State estimation for stochastic time varying systems with disturbance rejection. IFAC-PapersOnLine, 51(15):55–59, 2018. 18th IFAC Symposium on System Identification SYSID 2018.

[8] Eshwar Kuncham, Neha Aswal, Subhamoy Sen, and Laurent Mevel. Bayesian monitoring of substructures under unknown interface assumption. Mechanical Systems and Signal Processing, 193: 110269, 2023. ISSN 0888-3270.

[9] Manolis N. Chatzis, Eleni N. Chatzi, and Andrew W. Smyth. On the observability and identifiability of nonlinear structural and mechanical systems: OBSERVABILITY AND IDENTIFIABILITY OF NL STRUCT. AND MECH. SYSTEMS. Structural Control and Health Monitoring, 22(3):574–593, March 2015. ISSN 15452255. doi: 10.1002/stc.1690. URL https://onlinelibrary.wiley.com/doi/10.1002/stc.1690.

[10] Eric Walter and Yves Lecourtier. Global approaches to identifiability testing for linear and nonlinear state space models. Mathematics and Computers in Simulation, 24(6):472–482, 1982. ISSN 0378-4754. doi: https://doi.org/10.1016/0378-4754(82)90645-0. URL https://www.sciencedirect.com/science/article/pii/0378475482906450.

[11] Berit Floor Lund and Bjarne A. Foss. Parameter ranking by orthogonalization—applied to nonlinear mechanistic models. Automatica, 44(1):278–281, 2008. ISSN 0005-1098. doi: https://doi.org/10.1016/j.automatica.2007.04.006. URL https://www.sciencedirect.com/science/article/pii/S0005109807002336.

[12] Xinran Zhang, Chao Lu, and Ying Wang. Identifiability Analysis of Load Model Parameter Identification with Likelihood Profile Method. In 2018 IEEE Power & Energy Society General Meeting (PESGM), pages 1–5, Portland, OR, August 2018. IEEE. ISBN 978-1-5386-7703-2. doi: 10.1109/PESGM.2018.8586673. URL https://ieeexplore.ieee.org/document/8586673/.

[13] A.K. Singh and J. Hahn. On the use of empirical gramians for controllability and observability analysis. In Proceedings of the 2005, American Control Conference, 2005., pages 140–141 vol. 1, 2005. doi: 10.1109/ACC.2005.1469922.

[14] Christian Himpe. emgr—The Empirical Gramian Framework. Algorithms, 11(7):91, June 2018. ISSN 1999-4893. doi: 10.3390/a11070091. URL https://www.mdpi.com/1999-4893/11/7/91.

[15] Alejandro F. Villaverde, Antonio Barreiro, and Antonis Papachristodoulou. Structural Identifiability of Dynamic Systems Biology Models. PLOS Computational Biology, 12(10):e1005153, October 2016. ISSN 1553-7358. doi: 10.1371/journal.pcbi.1005153. URL https://dx.plos.org/10.1371/journal.pcbi.1005153.

[16] Alejandro F. Villaverde, Antonio Barreiro, and Antonis Papachristodoulou. Structural Identifiability Analysis via Extended Observability and Decomposition. IFAC-PapersOnLine, 49(26):171–177, 2016. ISSN 24058963. doi: 10.1016/j.ifacol.2016.12.121. URL https://linkinghub.elsevier.com/retrieve/pii/S2405896316327847.

[17] Johannes D. Stigter and Jaap Molenaar. A fast algorithm to assess local structural identifiability. Automatica, 58:118–124, 2015. ISSN 0005-1098. doi: https://doi.org/10.1016/j.automatica.2015.05.004. URL https://www.sciencedirect.com/science/article/pii/S0005109815001946.

[18] Oana-Teodora Chis, Julio R. Banga, and Eva Balsa-Canto. Structural Identifiability of Systems Biology Models: A Critical Comparison of Methods. PLoS ONE, 6(11):e27755, November 2011. ISSN 1932-6203. doi: 10.1371/journal.pone.0027755. URL https://dx.plos.org/10.1371/journal.pone.0027755.

[19] Hoon Hong, Alexey Ovchinnikov, Gleb Pogudin, and Chee Yap. Global identifiability of differential models. Communications on Pure and Applied Mathematics, 73, 01 2018. doi: 10.1002/cpa.21921.

[20] Sanjay Lall, Jerrold E. Marsden, and Sonja Glavaski. Empirical model reduction of controlled nonlinear systems. IFAC Proceedings Volumes, 32(2):2598–2603, 1999. ISSN 1474-6670. doi: https://doi.org/10.1016/S1474-6670(17)56442-3. URL https://www.sciencedirect.com/science/article/pii/S1474667017564423. 14th IFAC World Congress 1999, Beijing, Chia, 5-9 July.

[21] Christian Himpe. Empirical gramian framework (emgr). https://github.com/gramian/emgr/blob/main/py/emgr.py, 2023. Accessed: 2025-03-04.

[22] F. Nordtorp, E. E. Baş, C. Gomes, and G. Abbiati. A hybrid testing framework for wind turbine mechanical components. Journal of Physics: Conference Series, 2767(5):052046, jun 2024.